

# Geochemical Evolution of Intraplate Magmatism in the Paleo-Asian Ocean from the Late Neoproterozoic to the Early Cambrian

I. Yu. Safonova

*Institute of Geology and Mineralogy, Siberian Branch, Russian Academy of Sciences,  
pr. akademika Koptyuga 3, Novosibirsk, 630090 Russia*

*e-mail: inna@uiggm.nsc.ru*

Received 10 July, 2007; in final form 11 October, 2007

**Abstract**—A group of oceanic islands and/or seamounts (hereafter, paleoseamounts) was produced by oceanic hot-spot magmatism in the Late Proterozoic–Early Cambrian in the southwestern margin of the Paleo-Asian Ocean. They were accreted to the Kuznetsk–Altai island arc in the Late Cambrian and were subsequently incorporated during the closing of the paleocean into the accretionary complexes of the western part of the Altai–Sayan terrane (southwestern Siberia, Russia). The major- and trace-element compositions and Sr and Nd isotopic systematics of pillow lavas and basalt flows from the Kurai (600 Ma) and Katun' (550–530 Ma) paleoseamounts of Gorny Altai characterize the evolution of Hawaiian-type magmatism in the Paleo-Asian Ocean during that period. The obtained data show a significant change in lava composition between 600 and 550–530 Ma. The tholeiitic basalts of the Kurai Paleoseamount (600 Ma) from the southern part of Gorny Altai have lower incompatible element contents and higher  $^{147}\text{Sm}/^{144}\text{Nd}$  values compared with the younger tholeiitic and alkali basalts of the Katun' Paleoseamount (550–530 Ma), whose rocks are exposed in the northern Gorny Altai. The trace-element compositions of the Katun' lavas are similar to those of the Hawaiian tholeiites, and their  $^{147}\text{Sm}/^{144}\text{Nd}$  ratios are lower than those of the Kurai basalts. It was suggested that the older Kurai Paleoseamount was formed above a thinner oceanic lithosphere, i.e., closer to the paleospreading axis compared with the younger Katun' Paleoseamount. The observed temporal variations in the chemical and isotopic characteristics of lavas are probably related to differences in the degree of melting of the heterogeneous mantle owing to the different thickness of the oceanic lithosphere above which the Kurai and Katun' paleoseamounts were formed. During the Ediacaran, a plume developed beneath the younger and, consequently, thinner lithosphere of the Paleo-Asian Ocean. The higher degree of melting in the mantle column resulted in a more considerable contribution from the refractory depleted material of the upper mantle. After 50–70 Myr, i.e., in the Early Cambrian, the plume affected a thicker lithosphere, its mantle column became shorter, and the degree of melting was lower. Owing to this, the basaltic melt included more low melting point and incompatible element enriched materials from the lower mantle.

**DOI:** 10.1134/S0869591108050056

## INTRODUCTION

Intraplate hot-spot magmatism is considered to be the surficial manifestation of mantle plumes, which are columns of hot material ascending from the lower mantle (Morgan, 1971). The geochemical investigation of Precambrian and Paleozoic plume basalts provides insight into the mantle structure and composition during that time. Previous results on recent and ancient oceanic lavas have shown that the compositions of intraplate basalts of ocean islands and seamounts (OIB) are more diverse than the compositions of mid-ocean ridge basalts (MORB), which are produced by decompression melting of upper mantle peridotites (Hofmann, 1997; Reiners, 1998; etc.). A considerable literature exists on oceanic plume basalts; however, the nature of geochemical and isotopic variations in both young (basalts of the Emperor–Hawaii Seamount Chain; hereafter, EHC) and older intraplate lavas

remains obscure. Among the possible factors of deep mantle heterogeneity is the subduction of the oceanic lithosphere (Hofmann, 1997; Hofmann and White, 1982).

Primitive basalt magmas ascend from deep mantle sources to the surface without significant cooling and crystallization; consequently, data on their composition may provide information on the chemistry of mantle sources and the degree of partial melting of mantle materials. On the other hand, the initial composition of OIB may be changed at shallow depths by the influence of the oceanic lithosphere, proximity of a spreading center, and fractional crystallization. Seamount chains formed owing to the motion of oceanic plates over mantle plumes record changes in the composition of lavas erupted on the surface above a certain plume during a certain time period. Hence, the investigation of temporal variations in the chemistry of intraplate magmatism

allows us to estimate the influence of the oceanic lithosphere on the composition of intraplate lavas (Basu and Faggart, 1996; Dupuy et al., 1993). It is important to account for the influence of shallow processes on the composition of plume basalts during the interpretation of geochemical information. The analysis of data on many volcanic chains shows considerable variations in basalt composition in some of them, whereas other hotspots may produce lavas of relatively constant composition over a considerable time. For instance, the compositions of lavas from the Louisville hotspot track in the southern Pacific have only slightly changed within the past 70 Myr (Cheng et al., 1987), whereas the trace element and isotopic compositions of lavas erupted above the Hawaiian hotspot have shown considerable variations within the past 85 Myr (Regelous et al., 2003). Geochemical variations in intraplate basalts are usually assigned to their generation at different distances from a spreading axis and/or eruption onto the oceanic lithosphere of different age and, correspondingly, different thickness (Regelous and Hofmann, 1999; Regelous et al., 2003).

This paper reports the results of an investigation of the composition of basalts from the Kurai and Katun' paleoseamounts, whose fragments were detected in the Caledonian accretionary complexes of Gorny Altai (Fig. 1). Paleoislands and paleoseamounts were formed in the southwestern Paleo-Asian Ocean between 600 and 550–530 Ma. Our previous investigations (Safonova et al., 2004; Safonova, 2005) revealed significant differences in trace-element compositions between the lavas of the older Kurai Paleoseamount (600 Ma) and the younger Katun' Paleoseamount (550 Ma). Such geochemical variations are characteristic of many seamount chains younger than 85 Ma (Regelous et al., 2003; Ito and Mahoney, 2005). However, such investigations were never conducted for older oceanic ridges and seamounts, which are preserved in many accretionary belts of Russia's Far East, Japan, Australia, and Canada (Khanchuk et al., 1989; Voinova et al., 1994; Gordienko et al., 2007; Isozaki et al., 1990; Polat et al., 1999; Komiya et al., 2002). The problem is that the initial relationships of volcanics and associating sedimentary rocks were usually disturbed by tectonic processes, and it is very difficult to determine the age of basalts from various complexes and establish their relation to the evolution of a particular paleocean, a particular oceanic plate, and/or a particular hotspot. The Kurai (600 Ma) and Katun' (550 Ma) paleoseamounts are unique objects with well preserved primary relationships between basalts and sedimentary sequences, which can be used for reliable age determination. This provided an opportunity to correlate these objects with available paleogeodynamic reconstructions (see below).

Detailed geochemical and reconnaissance isotopic studies of lavas from both the paleoseamounts were carried out in order to characterize and interpret temporal variations in the composition of intraplate magma-

tism of the Paleo-Asian Ocean from the Late Proterozoic to the Early Cambrian.

## GEODYNAMIC SETTING

In Late Neoproterozoic time, a group of paleoislands and paleoseamounts existed in the Paleo-Asian Ocean, which was located between Siberia and eastern Gondwana and reached 4000 km in width (Zonenshain et al., 1990; Berzin et al., 1994; Dobretsov et al., 2005; McKerrow et al., 1992; Dobretsov et al., 1995; etc.). The closure of the Paleo-Asian Ocean produced several accretionary complexes, which are currently preserved in Gorny Altai. These complexes were formed during three main accretion–collision stages of paleocean evolution. The first stage included the Early Cambrian subduction of the oceanic plate, when the paleoislands and paleoseamounts were accreted to the extended Kuznetsk–Altai island-arc system in the southwestern part of the Siberian continent. The island arc was accreted together with the paleoseamounts to the Siberian continent during the second stage in the Late Cambrian–Early Ordovician owing to the continuing subduction, which was accompanied by folding and thrusting. The third stage included two events: the accretion of the Altai–Mongolia microcontinent of the Gondwana group to the Siberian continent and the collision of the Siberian and Kazakhstan continents. In the Late Paleozoic, the accretion–collision structure of the Siberian continent margin was disrupted by large dextral faults, which formed the peculiar mosaic–block structure of southern Siberia (Buslov et al., 2001, 2002). The Kurai and Katun' accretionary zones, which included the fragments of the Kurai and Katun' paleoseamounts, were formed during a single stage of Paleo-Asian Ocean evolution, the Middle Cambrian accretion of ocean islands and seamounts to the Kuznetsk–Altai island arc (Berzin et al., 1994; Simonov et al., 1994; Buslov et al., 2002).

Thus, the available geodynamic reconstructions suggest that the Kurai and Katun' paleoseamounts were formed within a single paleocean owing to hotspot activity. In general, intraplate magmatism had occurred in the Paleo-Asian Ocean from the Ediacaran to the Early Carboniferous (Safonova et al., 2004) and was related to the activity of either the Pacific (Maruyama, 1994) or the North Asian (Yarmolyuk et al., 2000) long-lived superplume.

## GEOLOGIC SETTING AND AGE OF BASALTS

Gorny Altai is a fold belt or terrane in the southwestern margin of the Siberian continent (Fig. 1). It has a complex tectonic structure formed via several stages of oceanic subduction; accretion of islands, seamounts, and microcontinents; and strike-slip faulting. The terrane includes tectonic units of different geodynamic origin: island-arc complexes, fragments of oceanic crust, accretionary wedges, deposits of fore-arc

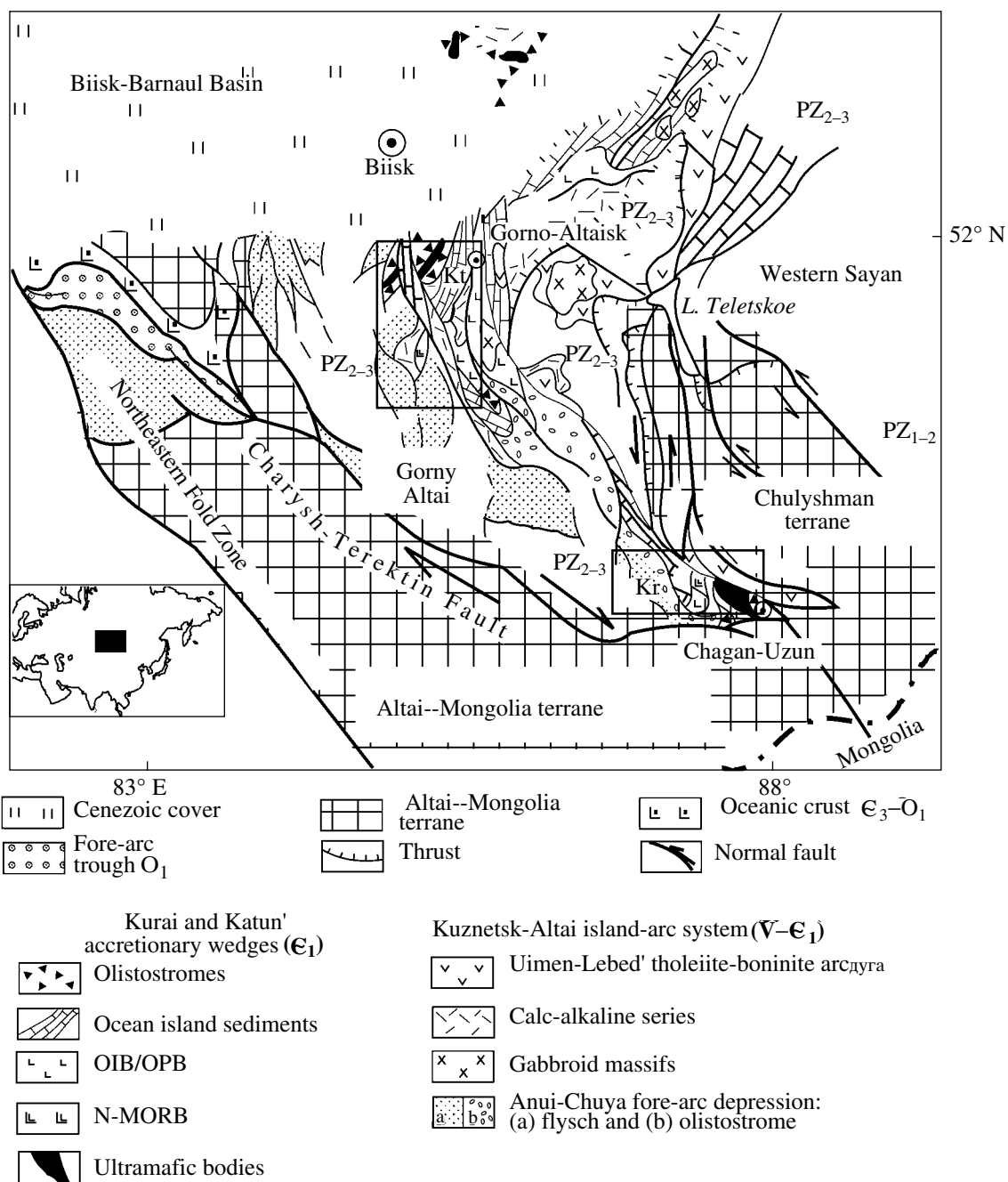


**Fig. 1.** Sketch map showing the geologic structure of Gorny Altai, modified after Buslov et al. (2001). Kr, Kurai Paleoseamount and Kt, Katun' Paleoseamount.

troughs, etc. (Buslov et al., 2001, 2002). The sequences containing fragments of paleoseamounts with intraplate basalts are structurally connected with the Kurai and Katun' accretionary complexes and alternate with thrust sheets of olistostromes and ophiolites. The Kurai Paleoseamount occurs in the Kurai accretionary complex and was previously called the Baratal Paleoseamount (Dobretsov et al., 2004; Buslov et al., 2001; Safonova et al., 2004). It is 70 × 20 km in size. The Katun' Paleoseamount of the Katun' accretionary com-

plex is located 200 km north of the Kurai Paleoseamount and is up to 120 km long and 40 km wide. Both paleoseamounts are made up of basalt lavas and chert-carbonate-terrigenous sequences. The geologic relationships of volcanogenic and sedimentary complexes in the paleoseamounts are briefly described below on the basis of published data (Dobretsov et al., 2004; Buslov et al., 2001, 2002; Safonova et al., 2004; Uchio et al., 2004; etc.) (Fig. 1).

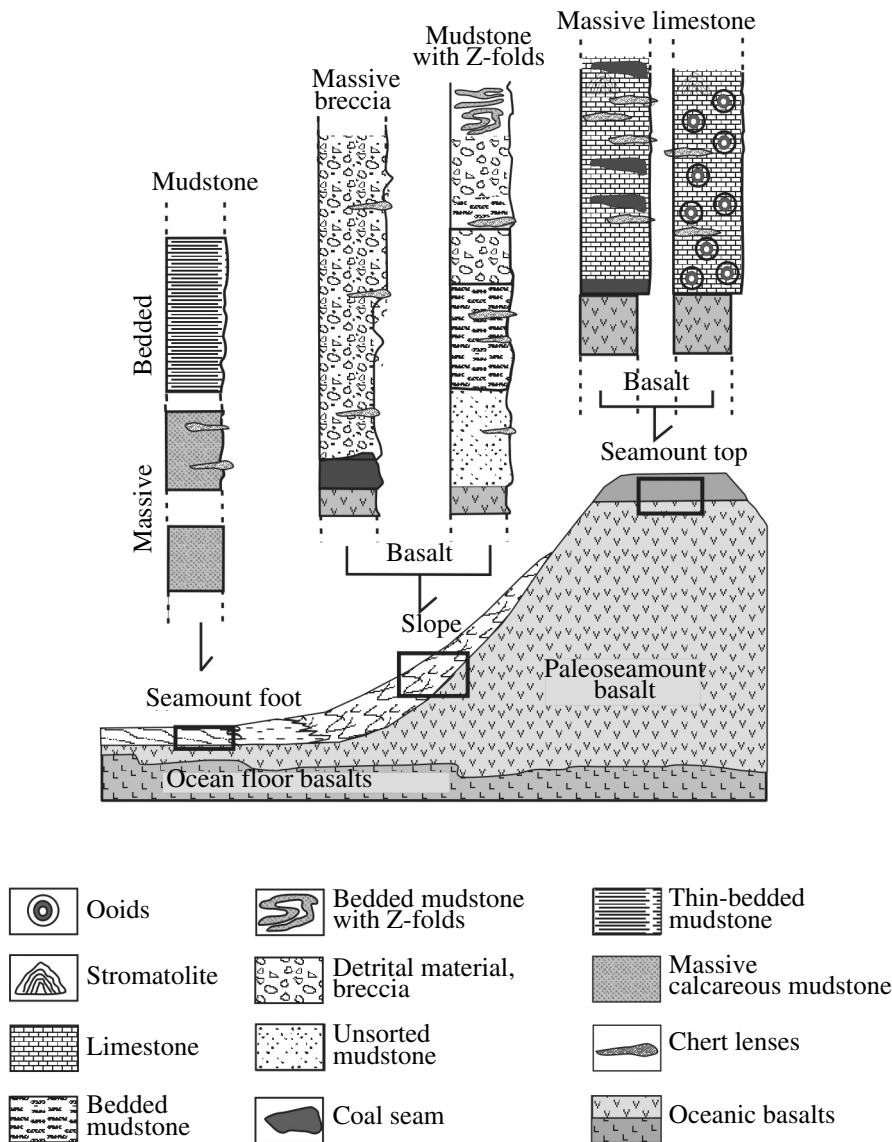


**Fig. 2.** Schematic reconstruction of the structure of an ocean island overlain by three types of carbonate rocks: massive limestones, bedded limestones, and carbonate breccias; modified after Isozaki et al. (1990).

Within the Kurai accretionary wedge in the southern part of Gorny Altai (Fig. 1), the paleoseamount complexes crop out fragmentarily in the area between the settlements of Chagan-Uzun and Kurai and are represented by the basalts of the main magmatic body, limestones of the carbonate cap, and slope-facies terrigenous rocks, as well as volcanosedimentary rocks of the paleoseamount base and ocean floor basalts (Buslov et al., 2002; Uchio et al., 2004). The paleoseamount is composed of three units, volcanogenic, volcanosedimentary, and sedimentary. The volcanogenic unit or the main igneous body consists of pillow lavas and flows of plagioclase and pyroxene–plagioclase phyric basalts altered under greenschist facies conditions. The igneous rocks comprise scarce interbeds and lenses of clas-

tic limestone, dolomite, chert, and volcanomictic sandstone (Fig. 2).

The volcanosedimentary unit (slope facies) includes bedded and massive limestones, limy mudstones, cherts, pillow lavas, and volcanic breccias and conglomerates interbedded with chloritized mudstones and volcanomictic sandstones. Their formation on the slopes of a paleoisland or paleoseamount is suggested by syndimentary folding (Z-folds), slump structures, brecciation, and variable thickness of sedimentary beds. The volcanosedimentary breccia consists of basalt, limestone, siltstone, and chert fragments embedded in a clay–carbonate–siliceous matrix (Fig. 2).

The sedimentary unit (carbonate cap of the island) is composed of carbonate and siliceous rocks. The carbonate rocks are massive and bedded gray limestones

and carbonate breccias. The limestones often conformably overlie pillow lavas. The massive limestones contain chert nodules, interbeds and lenses of black limestone, stromatolites, and ooids. The bedded micritic limestones are partly dolomitized, associate with limestone breccias, and intercalate with cherts. They often show slump structures. Both of the limestone varieties are free of coarse-grained terrigenous material (Fig. 2).

The Katun' accretionary complex is located in the northern part of Gorny Altai, south of Gorno-Altai (Fig. 1). It is composed of five tectonic units or sheets and includes basalts, limestones, cherts, mudstones, and sandstones. Within each sheet, lavas are conformably overlain by limestones with thin interbeds and lenses of chert and mudstone with sandstone and chert lenses. The basalts occur as massive and pillow lavas, lava breccias, dikes, and sills and often contain limestone beds and blocks. The basalt-sedimentary unit includes three rock groups, which were previously parts of a single paleoisland or paleoseamount: (1) basalt-siliceous-clay assemblage of the paleoseamount base; (2) brecciated carbonate-chert-clay-basalt slope facies; and (3) massive and bedded rocks of the carbonate cap. The bedded limestones rest directly on the lavas and contain chert interbeds (Dobretsov et al., 2004).

The above descriptions indicate that the basalts of both the structures are closely associated with three types of sediments: carbonate cap, slope facies (with synsedimentary folding and slump structures), and sediments of the paleoseamount base (Fig. 2). The general consensus among the investigators of Gorny Altai is that the Kurai and Katun' basalts were formed in an oceanic environment (Berzin et al., 1994; Gibsher et al., 1997; Dobretsov et al., 2004; Buslov et al., 2001; Ota et al., 2007; etc.). This is supported by the association of basalts with oceanic sediments (cherts) and ophiolitic rocks and alternation of basalts with massive limestones and slope-facies sediments. Of particular importance is that the basalts are overlain by the limestones of the carbonate cap, whose thickness is estimated as 500 m (Uchio et al., 2004).

The Ediacaran (Late Vendian) age of the limestones of the Kurai Paleoseamount ( $598 \pm 25$  Ma) was constrained by the Pb-Pb isochron method at the Tokyo Institute of Technology (Uchio et al., 2004). The slope deposits overlying the basalts of the Katun' paleoseamount contain remains of microphytolites, calcareous algae, and siliceous sponge spicules, which indicated an Early Cambrian age (550–530 Ma) for the sedimentary rocks (Terleev, 1991; Postnikov and Terleev, 2004). The Katun' accretionary wedge is stratigraphically overlain by the island-arc rocks of Sanashtyngol (Late Cambrian) age (Repina and Romanenko, 1978), which supports the aforementioned age estimates. These pieces of evidence allow us to accept ages 600 Ma for the Kurai basalts and 550–530 Ma for the Katun' basalts.

Thus, both the paleoseamounts have similar structures in terms of relationships between basalts and oceanic stratigraphic units: siliceous deposits of the paleoseamount base, slope-facies terrigenous sediments, and shallow-water carbonate-cap sequences. The ages of the paleoseamounts differ by 50–70 Myr. Based on the combined geological, geochronological, and geochemical data, we believe that the Kurai and Katun' paleoseamounts were produced by intraplate magmatism, which was related to the activity of a mantle plume in the Paleo-Asian Ocean.

## ANALYTICAL METHODS

The basalts of the Kurai and Katun' paleoseamounts were sampled northeast of the Kurai settlement and south of Gorno-Altai, respectively (Fig. 1), from the least deformed and altered flows and dikes with the minimum amounts of veinlets and amygdules. The samples were ground in an agate mortar. The total of major oxides in the analyses was  $100 \pm 1$  wt %.

The major and trace elements were analyzed at the Institute of Geology and Mineralogy, Siberian Branch, Russian Academy of Sciences. Major element contents were measured by XRF using a Nauchpribor spectrometer following State Standard (GOST) 41-08-212-82 of the Ministry of Geology of the USSR. The contents of trace elements, including rare earth elements (REE), were determined by INAA using Ge detectors for gamma-rays with energies from 30 to 2000 keV. The high field strength elements (HFSE) and large ion lithophile elements (LILE) were analyzed by SF XRF using the methods described by Phedorin et al. (2000). Some samples were also analyzed by ICP-MS using a Finnigan Element instrument.

The isotopic compositions of Sm, Nd, Sr, and Rb were analyzed at the Vernadsky Institute of Geochemistry and Analytical Chemistry, Russian Academy of Sciences using a TRITON mass spectrometer. The concentrations of Rb, Sr, Sm, and Nb were determined by the isotope dilution method. The samples were decomposed in an HF + HNO<sub>3</sub> mixture at a temperature of 200°C for two days using titanium autoclaves with Teflon inserts. The sample was spiked before decomposition with a mixed <sup>85</sup>Rb + <sup>84</sup>Sr tracer. The separation of Rb, Sr, and all rare earth elements was carried out by ion exchange chromatography using Teflon columns with 3.5 ml of Dowex 50 × 8 resin and 2.3 N HCl as an eluent. Nd and Sm were separated on Eichrom Ln.spec columns by stepwise elution with 0.5 N and 0.75 N HCl, respectively. The long-term precision of isotopic analysis was controlled using international standards: SRM-87 for Sr and La Jolla for Nd. The obtained isotopic ratios are <sup>87</sup>Sr/<sup>86</sup>Sr =  $0.710256 \pm 18$  ( $N = 21$ ) and <sup>143</sup>Nd/<sup>144</sup>Nd =  $0.511843 \pm 11$  ( $N = 19$ ).

## PETROGRAPHY

The volcanics of the Kurai accretion wedge are petrographically rather uniform. Porphyritic and aphyric basalts are most common. Both massive and amygdaloidal varieties were observed. The amygdules are filled with calcite and chlorite. The phenocrysts are plagioclase and clinopyroxene. The groundmass has a variolitic or hyalopilitic texture. The rocks underwent greenschist-facies metamorphism.

The volcanic rocks of the Katun' accretion wedge show a massive or, occasionally, amygdaloidal structure and an aphyric or fine-grained porphyritic texture. The most abundant rocks are diabases, basalts, and pyroxene and plagioclase porphyrites. The rocks underwent extensive chloritization, amphibolization, and albitization. The groundmass shows an intersertal texture and contains feldspar laths and microlites.

## PETROCHEMISTRY AND GEOCHEMISTRY OF BASALTS

The major- and trace-element compositions of basalts from the Kurai and Katun' paleoseamounts were considered to some extent by Dobretsov et al. (2004), Safonova (2005), and Safonova et al. (2004) and are shown in Figs. 3–6. The samples are mainly tholeiitic and subalkali basalts. As the initial composition of most of the samples was modified by postmagmatic processes, the concentrations of mobile elements (i.e., LILE, Fe, and Mn) cannot be regarded as initial. Secondary calcite, quartz, and chlorite were observed in voids in most of the samples. Clinopyroxene and plagioclase grains are partly replaced by chlorite, amphibole, saussurite, calcite, and iron hydroxides, which also affected the contents of Ca, K, Na, and P. The basalts of the two paleoseamounts are almost identical in major-element contents, but distinctly different with respect to incompatible trace elements (Figs. 3–6).

*Kurai Paleoseamount (~600 Ma)*

Sixteen basalt samples (4.3–7.9 wt % MgO) were collected at the Kurai area. They have diverse petrographic textures and include fine- and medium-grained, amygdaloidal, and porphyritic varieties. The moderately and strongly altered clinopyroxene and clinopyroxene–plagioclase aphyric basalts show a relatively high scatter in Mg# and Fe<sub>2</sub>O<sub>3</sub> at a relatively narrow range of SiO<sub>2</sub> (Table 1, Fig. 3): SiO<sub>2</sub> = 47–52 wt %, Al<sub>2</sub>O<sub>3</sub> = 12.9–17.9 wt %, Fe<sub>2</sub>O<sub>3</sub> = 7.5–14.9 wt %, Mg# = 66–36, and Ni = 7–96 ppm. There is no correlation between Ti/Zr and Mg#. The contents of TiO<sub>2</sub> and P<sub>2</sub>O<sub>5</sub> range from 0.43 to 2.42 wt % and from 0.08 to 0.58 wt %, respectively (Table 1). Compared with island-arc tholeiites (Frolova and Burikova, 1997), the Kurai metabasalts are depleted in K, Rb, and Ba and slightly enriched in Zr, Nb, U, Th, and Hf and show considerable variations in Ba/Rb ratio (2–104, averaging 27.6), which is higher than the oceanic basalt value

(11.6). This suggests that the contents of mobile alkalis were modified during postmagmatic processes. The LOI values in the majority of samples are higher than 2 wt % (Table 1).

Based on the analysis of the distribution of REE contents and Zr/Nb ratios, transitional and enriched groups were distinguished among the basalts of the Kurai Paleoseamount. The rocks of the former, most abundant group show transitional compositional characteristics and  $(Zr/Nb)_{av} = 35$  (Table 1). The transitional varieties display flat REE patterns without any significant enrichment of light REE (LREE) and a relatively high general level of REE contents:  $La_N = 45–8.0$ ,  $(La/Yb)_N = 0.74–2.37$ ,  $(La/Sm)_N = 0.7–2.61$ , and  $(Gd/Yb)_N = 0.66–1.52$ . Compared with MORB compositions, they have higher incompatible element contents (Figs. 3, 4); higher incompatible/compatible element ratios (for instance,  $Zr/Y = 2.4–2.77$  as compared with 2.1–2.3 in MORB); lower Ni/Co, Cr/V, and Al<sub>2</sub>O<sub>3</sub>/TiO<sub>2</sub> (6–7 on average); and higher LREE, Th/Ta, and Rb/Sr values, which is in agreement with the data of Frolova and Burikova (1997) (Table 1). Their REE patterns are similar to those of the Nauru and Ontong Java plateau basalts (Safonova et al., 2004) and lavas from the Detroit Seamount of the EHC (Fig. 5a).

Enriched basalts are less common (samples C-80a-04 and 96-56-1 in Table 1), and their geochemical characteristics are similar to those of typical OIB: elevated contents of LREE [ $La_N = 30.0–36.8$  and  $(La/Yb)_N = 1.96–4.8$ ] and low Zr/Nb ratios (26 and 8). The  $(La/Sm)_N$  ratio ranges from 1.33 to 1.67, and  $(Gd/Yb)_N$ , from 1.31 to 2.21 (Fig. 5a, Table 1).

Both the transitional and enriched basalts of the Kurai area occur as fragments of sheets in fold structures; hence, their primary geologic relations cannot be determined. The enriched and transitional varieties have similar Al<sub>2</sub>O<sub>3</sub> contents (on average, 14.7 and 13.4 wt %, respectively), but the transitional basalts show higher Al<sub>2</sub>O<sub>3</sub>/TiO<sub>2</sub> (6.5 and 5.5), lower Ni contents (29 and 105 ppm), and less fractionated REE patterns [ $(La/Yb)_N$  of 1.7 and 3.4] (average values are given; Table 1, Fig. 5a). The basalts of both groups are moderately depleted in Th relative to La,  $(Th/La)_{pm} = 0.35–0.69$ . Compared with the younger tholeiites of the EHC (<42 Ma), the Kurai basalts have lower incompatible element contents (Fig. 4) and are similar in composition to the older lavas of the Meiji (85 Ma) and Detroit (81 Ma) seamounts (Regelous et al., 2003).

Most of the primitive-mantle normalized multielement diagrams exhibit a negative Nb anomaly and enrichment of HFSE and REE relative to MORB (Fig. 6a). Some transitional basalts have moderate depletion of Nb and Th relative to La:  $(Nb/La)_{pm} = 0.2–0.85$  and  $(Th/La)_{pm} = 0.3–0.9$  (Table 1), which distinguishes them from alkali basalts formed in continental rift environments (with characteristic Th enrichment) and typical OIB (with characteristic Nb enrichment) (Hofmann, 1997). Other transitional basalts

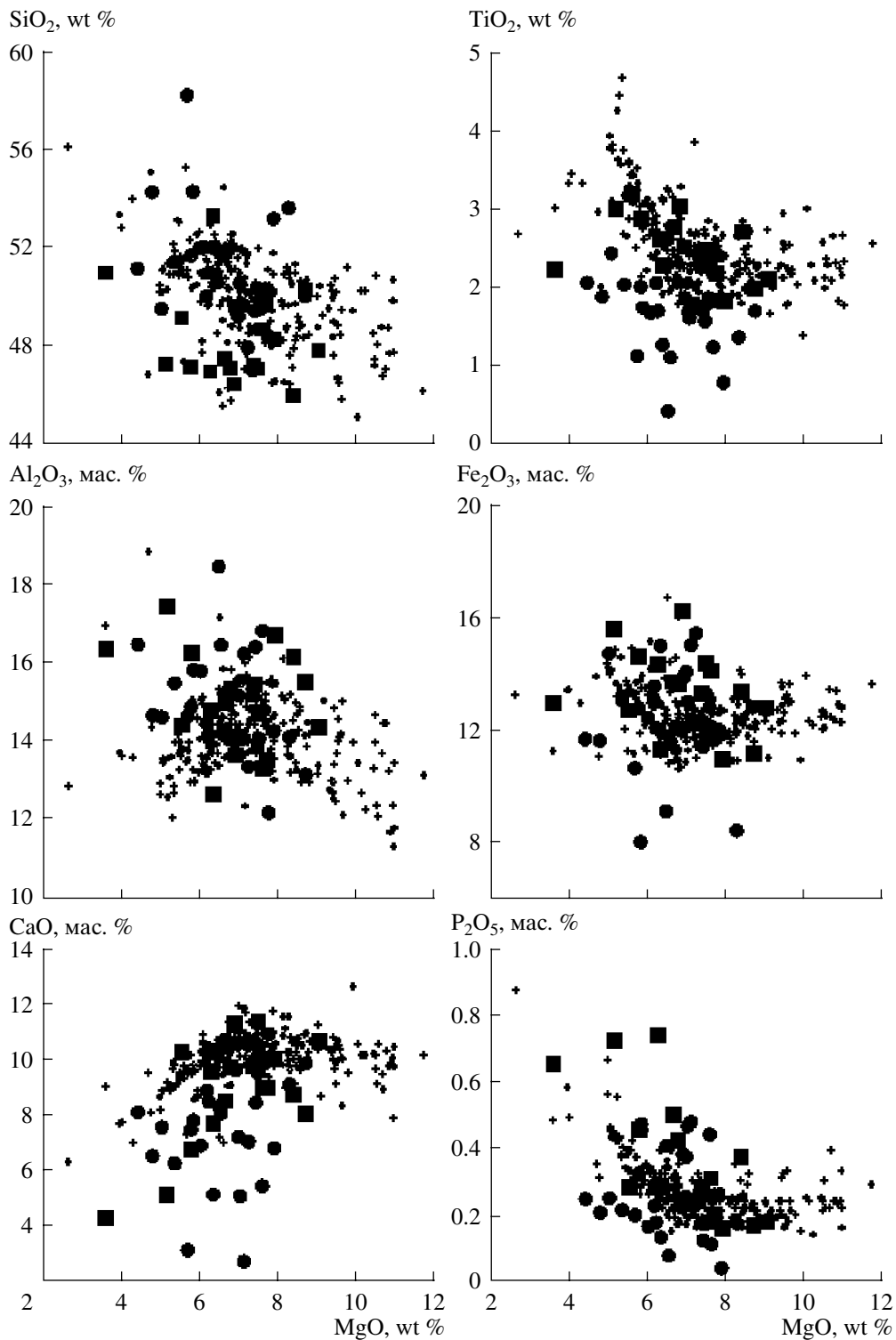


**Fig. 3.** Binary diagrams major oxide–MgO for the basalts of the Kurai (circles) and Katun' (squares) paleoseamounts. Also shown for the sake of comparison are the tholeiites of the Emperor–Hawaii volcanic chain (crosses) (Regelous et al., 2003 and the GEO-ROC database, <http://georoc.mpch-mainz.gwdg.de>).

show minor positive anomalies of La or Ce relative to Th and Nb, i.e., an inflection of curves upward at Th, Nb, and La,  $(\text{Nb/La})_{\text{pm}} = 0.2\text{--}1.5$  (Fig. 6a, Table 1). All of the samples with a negative Nb anomaly have

$(\text{La/Nb})_{\text{pm}} < (\text{Th/Nb})_{\text{pm}}$ , which rules out their crustal contamination or suprasubduction origin as a reason for the observed low Nb contents. Enriched basalt sample C-80a-04 shows a pronounced Nb enrichment relative

to Th and La (Fig. 6a). Similar multicomponent patterns were observed in many Phanerozoic transitional and alkali basalts of ocean islands, as well as in Proterozoic and even Archean volcanics interpreted as OIB (Sun and McDonough, 1989; Stern et al., 1995; Polat et al., 1999; Komiya et al., 2002).

#### *Katun' Paleoseamount (~550 Ma)*

Fourteen samples from the Katun' area are mostly tholeiitic and, occasionally, alkali basalts with porphyritic phenocrysts of pyroxene and plagioclase and contain 3.5–8.7 wt % MgO. Their compositional fields overlap the compositions of Hawaiian tholeiites in almost all binary MgO–major element diagrams (Fig. 3).

In the Katun' lavas, SiO<sub>2</sub> ranges from 47 to 52 wt %, Al<sub>2</sub>O<sub>3</sub> = 12.95–16.8 wt %, Fe<sub>2</sub>O<sub>3</sub> = 9.4–15.5 wt %, Mg# = 39.5–60.8, and Ni = 7–96. There is also no correlation between Ti/Zr and Mg#, and TiO<sub>2</sub> and P<sub>2</sub>O<sub>5</sub> contents are 1.4–2.9 wt % and 0.14–0.72 wt %, respectively (Table 2), which are higher than those of the Kurai lavas. In general, the abundances of immobile trace elements in the Katun' lavas are similar to those in the respective rock types from the young seamounts of the EHC and the Hawaiian Islands (Sun and McDonough, 1989; Hofmann and Jochum, 1996; Regulous et al., 2003). Compared with the older Kurai lavas, the Katun' rocks are enriched in LREE and HFSE (Zr, Nb, Th, and Hf) (Figs. 5, 6). Their Ba/Rb ratio also varies considerably from 2 to 104, indicating changes in primary geochemical characteristics during postmagmatic alterations (Table 2).

The Katun' lavas have lower Zr/Nb ratios compared with those of the Kurai Paleoseamount (3–6 versus 26–35). They show LREE enriched patterns with average La<sub>Ncp</sub> = 52.8 and (La/Yb)<sub>N</sub> = 2.16–8.54. There is no Eu anomaly, and the REE are moderately fractionated: (La/Sm)<sub>N</sub> = 1.3–3.65 and (Gd/Yb)<sub>N</sub> = 1.4–3.4 (Fig. 5b).

The primitive mantle-normalized patterns of trace elements for the Katun' lavas display positive Nb anomalies and slight negative Zr–Hf anomalies (Fig. 6b). Similar to the Kurai rocks, the Katun' basalts are depletion in Th relative to La, (Th/La)<sub>pm</sub> = 0.43–0.71 (Table 1, Fig. 6b). Nonetheless, the Katun' lavas show more pronounced negative Nb anomalies relative to La and Th: (Nb/La)<sub>pm</sub> = 1.06–2.87 and (Nb/Th)<sub>pm</sub> = 1.92–4.75 compared with the Kurai lavas (Fig. 6). Negative Y anomalies were observed in some samples of Katun' lavas, which could be related to the crystallization of garnet in the residue, because such samples also show rather fractionated heavy REE patterns, (Gd/Yb)<sub>n</sub> = 2.1–3.4 (Table 2). In general, the geochemical characteristics of this group support the suggestion that the melts were derived from an independent source enriched in REE, Nb, and Ti.

Thus, compared with the older basalts of the Kurai Paleoseamount (600 Ma), the Katun' basalts (550 Ma)

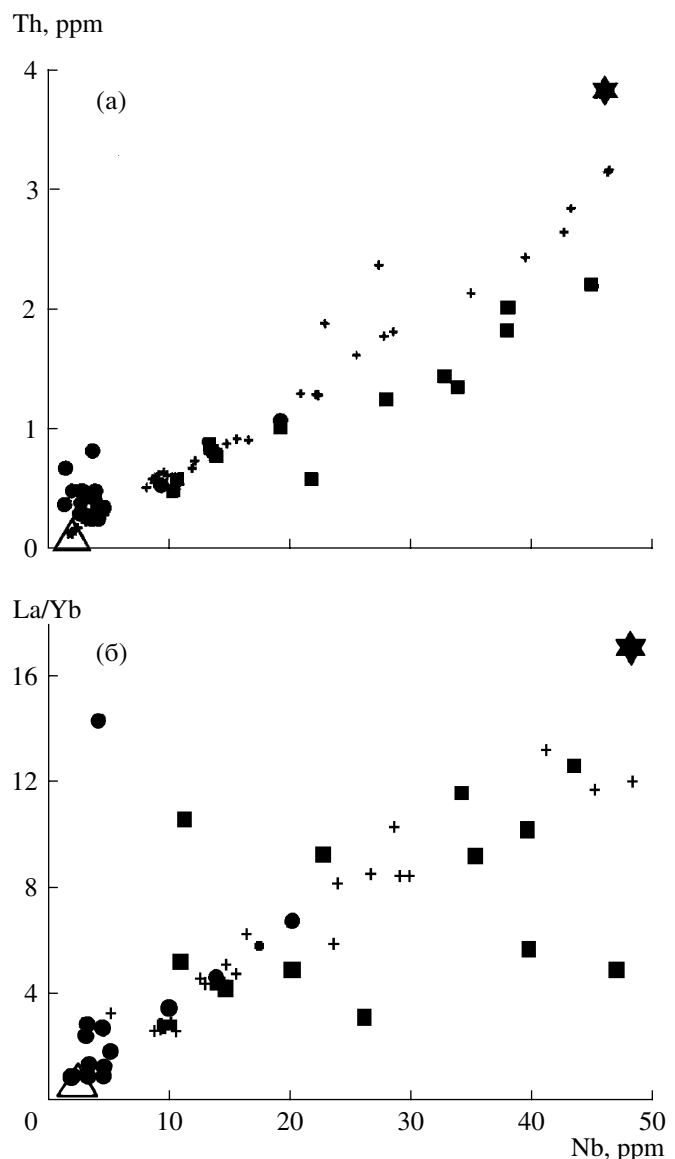


**Fig. 4.** Variations in (a) Th and (b) La/Yb as a function of Nb content. The triangle is MORB, and the asterisk is OIB after Sun and McDonough (1989). Other symbols are the same as in Fig. 3.

are enriched in Ti and incompatible elements, i.e., similar in composition to the lavas of the young EHC seamounts (<42 Ma) and tholeiites of the Hawaiian Islands (Figs. 4–6). The contents of some incompatible elements in the Katun' lavas (for instance, Th) are lower than in typical OIB (Sun and McDonough, 1989) but similar to those in the EHC lavas (Figs. 4–6). The contents of HREE (from Gd to Lu) and REE and multielement patterns are similar to those of the young EHC tholeiites (Figs. 5, 6). In general, the trace element compositions of the tholeiites of the Katun' Paleoseamount are identical to those of the majority of intraplate tholeiites described by Sun and McDonough (1989), Hofmann (1997), etc.

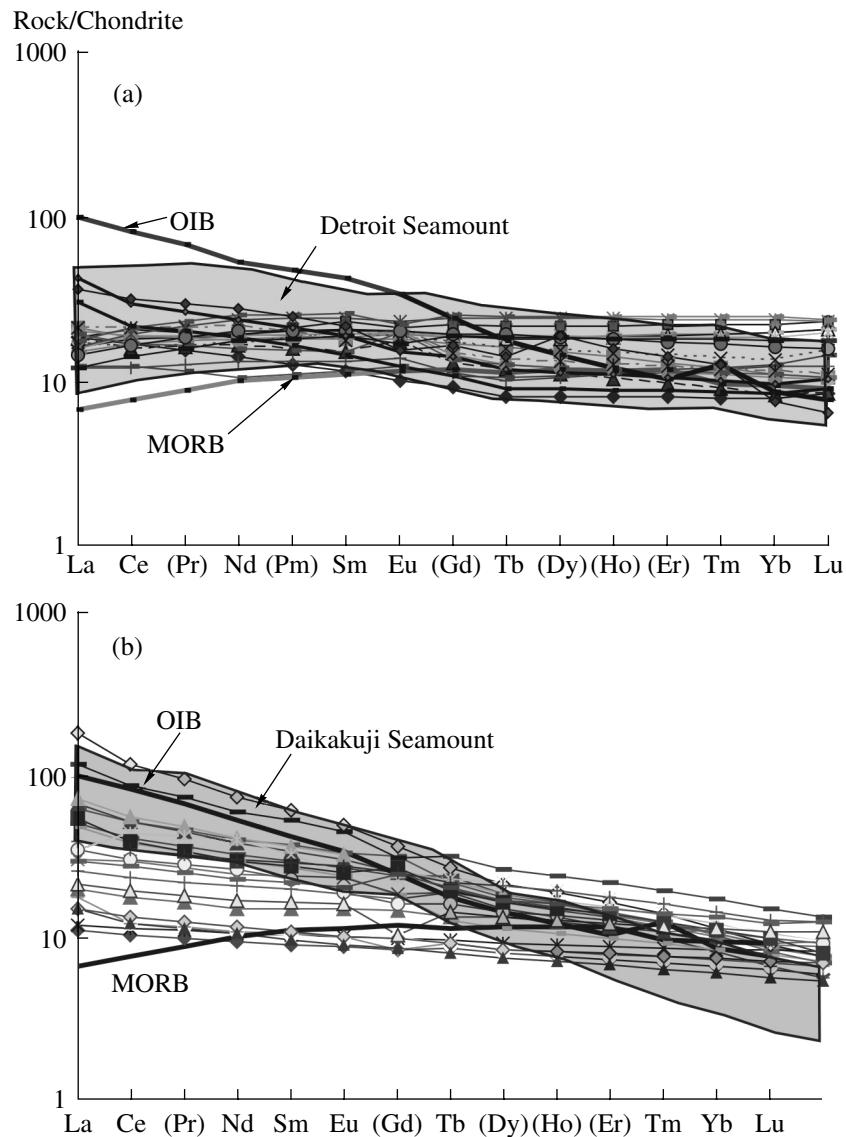


**Fig. 5.** Chondrite-normalized (Sun and McDonough, 1989) distribution patterns of rare earth elements in the basalts of the (a) Kurai and (b) Katun' paleoseamounts. The shaded fields show the compositions of the (a) Detroit and (b) Daikakuji seamounts of the EHC.

#### SR AND ND ISOTOPIC SYSTEMATICS

The Sr and Nd isotope ratios of lavas from the Kurai (four samples) and Katun' (one sample) paleoseamounts were corrected for radioactive decay since the time of their eruption, and the  $\epsilon_{\text{Sr}}$  and  $\epsilon_{\text{Nd}}$  values are given relative to CHUR.

The general range of  $\epsilon_{\text{Nd}}$  values for the Kurai basalts (transitional and enriched) is from +7.8 to +8.1, which is close to the values of the EHC lavas (Fig. 7) (Regelous et al., 2003). In contrast, the initial  $\epsilon_{\text{Sr}}$  values of the Kurai tholeiites (3.49–13.46) are much higher than those of tholeiites from the EHC and Hawaiian Islands. In the  $\epsilon_{\text{Sr}}-\epsilon_{\text{Nd}}$  diagram (Fig. 7), the points of the Kurai basalts cluster within the upper right (forbidden) quadrant and, in part, near the field of PREMA (HIMU)-type sources and form an array extending

along the  $x$  axis. Mahoney et al. (1998) described similar relations in ancient leached (i.e., strongly altered) basalts and assigned this effect to the incorporation of nonmagmatic Sr into the crystal lattice during plagioclase albitization. Other authors also suggested that such considerable  $^{87}\text{Sr}$  enrichments could result from either contamination with terrigenous sediments subducted into the mantle or postmagmatic alteration of basalts, in particular, isotopic exchange between Sr-rich seawater and basalt magma erupted on the seafloor (Dickin, 1995). We explain the high  $\epsilon_{\text{Sr}}$  values of the Kurai basalts by their postmagmatic alteration under seafloor conditions. When projected onto the  $y$ -axis, the compositions of the Kurai lavas fall within the segment of Hawaiian lavas. The  $\epsilon_{\text{Sr}}$  values of the Kurai lavas are positively correlated with K, Sr, and Rb con-

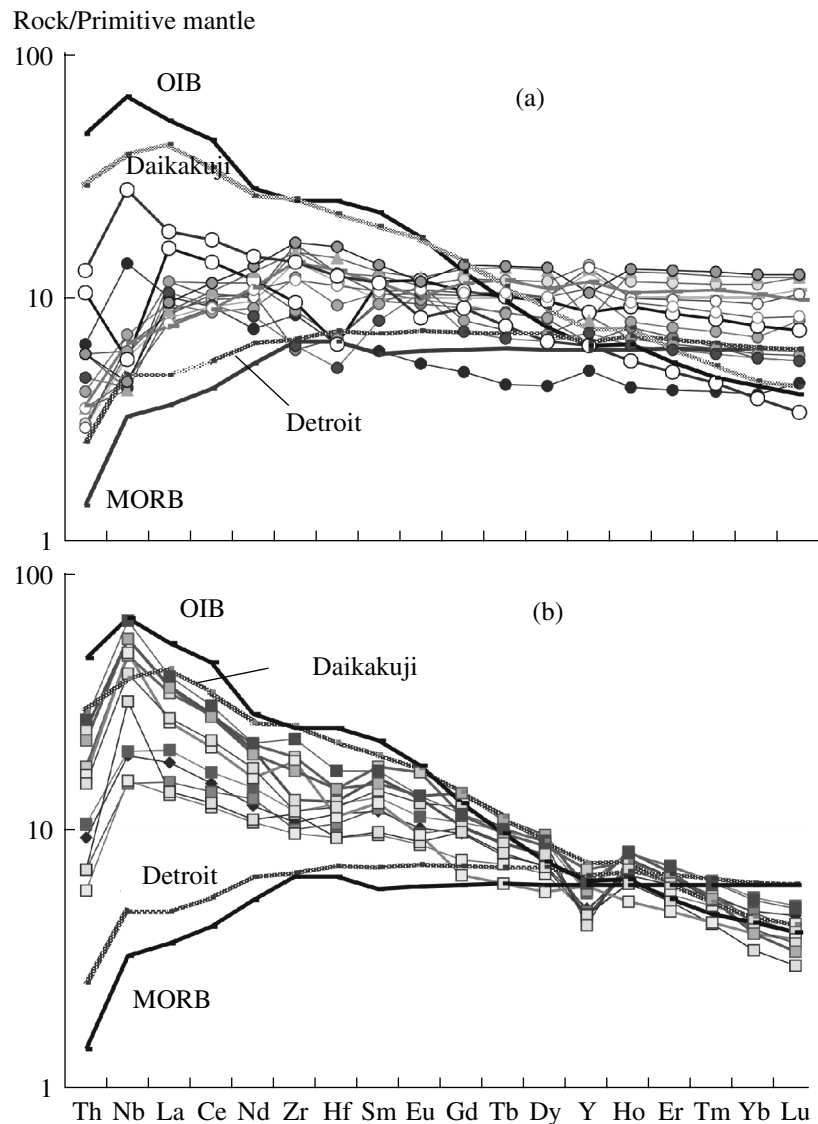


**Fig. 6.** Multi-element diagrams normalized to the primitive mantle composition (Sun and McDonough, 1989) for the basalts of the (a) Kurai and (b) Katun' paleoseamounts. For the sake of comparison, also shown are the compositions of basalts from the Detroit and Daikakuji seamounts of the EHC.

tents, which indirectly supports the suggestion that secondary alterations are responsible for the high  $\epsilon_{\text{Sr}}$  values. The Sr and Nd isotopic compositions of similar ancient oceanic basalts from the Altai–Sayan fold belt reported by Yarmolyuk and Kovalenko (2003) and altered oceanic basalts from the Aruba Plateau (White et al., 1999) also plot within the upper right (forbidden) quadrant of the  $\epsilon_{\text{Nd}}-\epsilon_{\text{Sr}}$  diagram. Thus, if the influence of postmagmatic processes is eliminated, the compositions of the Kurai basalts plot within the field of Hawaiian lavas in the Sr–Nd isotopic diagram (Fig. 7).

The tholeiite of the Katun' Paleoseamount has initial isotopic ratios corresponding to higher  $\epsilon_{\text{Sr}}$  (–5.66) and lower  $\epsilon_{\text{Nd}}$  (+5.3) compared with the average EHC values (Regelous et al., 2003). Nonetheless, it falls within the field of overlap between the compositions of

shield and postshield tholeiites from the EHC (Fig. 7). There is no direct correlation between isotope ratios ( $^{143}\text{Nd}/^{144}\text{Nd}$  and  $^{87}\text{Sr}/^{86}\text{Sr}$ ) and the degree of LREE enrichment; hence, it can be supposed that the source was enriched shortly before the derivation of basaltic melt.

#### REASONS FOR GEOCHEMICAL VARIATIONS IN THE LAVAS OF THE KURAI AND KATUN' PALEOSEAMOUNTS

The model of formation of the Kurai and Katun' paleoseamounts and reasons for the geochemical variations of their basalts are discussed assuming that the Ediacaran–Early Cambrian intraplate magmatism of the Paleo-Asian Ocean was produced by a single

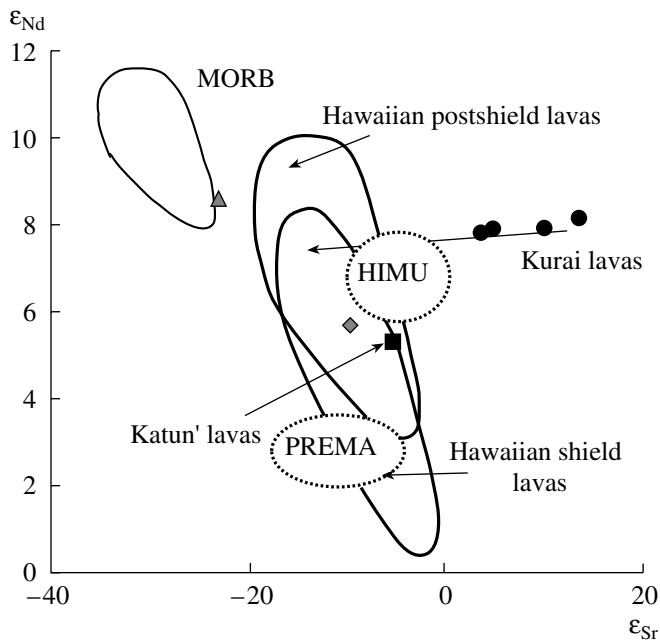


**Fig. 7.** Diagram  $\epsilon_{Sr}$ - $\epsilon_{Nd}$ . The fields of MORB and Hawaiian lavas are given after the GEOROC database (<http://georoc.mpch-mainz.gwdg.de>). EHC seamounts: Detroit (triangle, 85 Ma) and Daikakuji (diamond, 42 Ma) (Regelous et al., 2003). Other symbols are the same as in Fig. 3.

hotspot operating within a single oceanic plate. This assumption is based on the following considerations: (1) the age range of formation of the Kurai and Katun' paleoseamounts is 50–70 Myr, from 600 to 550–530 Ma (Postnikov and Terleev, 2004; Uchio et al., 2004); (2) it is considerably smaller than the maximum age of the oceanic crust, which is constrained by paleomagnetic and stratigraphic data as 160 Ma (Pitman and Talwani, 1972; Berger and Winterer, 1974); (3) the 50–70 Myr interval is comparable to the age of the longest lived Hawaiian and Kerguelen hotspots (85 and 90 Ma, respectively; Regelous et al., 2003; Frey and Weis, 1995); (4) both paleoseamounts show similar structures and lithologies of associating sedimentary sequences (Dobretsov et al., 2004), which may indicate their formation under similar geodynamic conditions; and (5) the basalt–sediment sequences of both the paleoseamounts are structurally related to a single accretionary prism of the Kuznetsk–Altai island arc (Berzin et al., 1994; Simonov et al., 1994; Buslov et al., 2002).

Figure 8 compares the compositions of lavas from the Kurai (600 Ma) and Katun' (550 Ma) paleoseamounts using the approach of Regelous et al. (2003), who compared the older (85–45 Ma) lavas of the EHC with the younger (<42 Ma) lavas of the Hawaiian Islands. The difference between the oldest lavas of the EHC (Meiji and Detroit seamounts) and the EHC rocks with ages of less than 42 Ma and young Hawaiian lavas is similar to that between the tholeiites of the older Kurai Paleoseamount (600 Ma) and the younger Katun'

Paleoseamount. The Kurai lavas have lower contents of incompatible elements (Nb, La, and Th), lower ratios of these elements, and higher  $\epsilon_{Nd}$  values compared with the younger Katun' rocks. The average La/Yb and Gd/Yb ratios and Th and Nb contents in the Kurai lavas are lower than those of the Katun' rocks (Fig. 8), and the trace-element composition of the former is similar to that of the Meiji (85 Ma) and Detroit (81 Ma) lavas (Figs. 5a, 6a). The trace-element characteristics of the Katun' lavas are similar to those of the Hawaiian lavas and the youngest EHC basalts from the Daikakuji Seamount (Figs. 5b, 6b) (Regelous et al., 2003).

The combined geological, lithological, and geochemical data provide compelling evidence that both the older depleted lavas of the Kurai zone and the enriched basalts of the Katun' zone were related to intraplate plume magmatism (Dobretsov et al., 2004; Buslov et al., 2001; Safonova et al., 2004). Therefore, the considerable variations in the composition of plume basalts of the Paleo-Asian Ocean from two accretionary complexes of Gorny Altai require further discussion. There are only a few isotopic data for the Gorny Altai basalts, which complicates the reliable identification of their mantle source. Therefore, some of our conclusions were based on the available results of the investigation of EHC lavas (Regelous et al., 2003 and references therein).

By analogy with previous models, temporal variations in the intraplate magmatism of the Paleo-Asian Ocean must be considered for the interpretation of the more depleted trace-element and Nd isotope compositions of the older tholeiites from the Kurai Paleoseamount compared with the younger Katun' tholeiites. Keller et al. (2000) supposed that a mantle melting column beneath a younger (i.e., thinner) oceanic lithosphere ascends to shallower levels (it is merely taller); consequently, intraplate lavas erupted onto a thinner lithosphere are formed at higher degrees of melting compared with magmas derived beneath a thicker lithosphere. The reason is that the thicker overlying oceanic lithosphere restricts the ascent of the mantle column during decompression melting. Consequently, the taller the melting column, the higher the degree of melting (Ellam, 1992; Haase, 1996).

In addition to the degree and depth of melting, trace-element characteristics are also affected by the amount of melt produced within the garnet stability field (Ellam, 1992; Haase, 1996). The older Kurai tholeiites have lower La/Sm and higher Lu/Hf ratios compared with the Katun' rocks (Figs. 5, 9). The trace element composition of Kurai lavas suggests that they could be derived beneath a thinner (younger at that time) lithosphere at relatively high degrees of mantle melting and moderate pressures within the spinel stability field (Fig. 9). In contrast, the Katun' lavas were formed at lower degrees of melting and higher pressures within the garnet stability field.

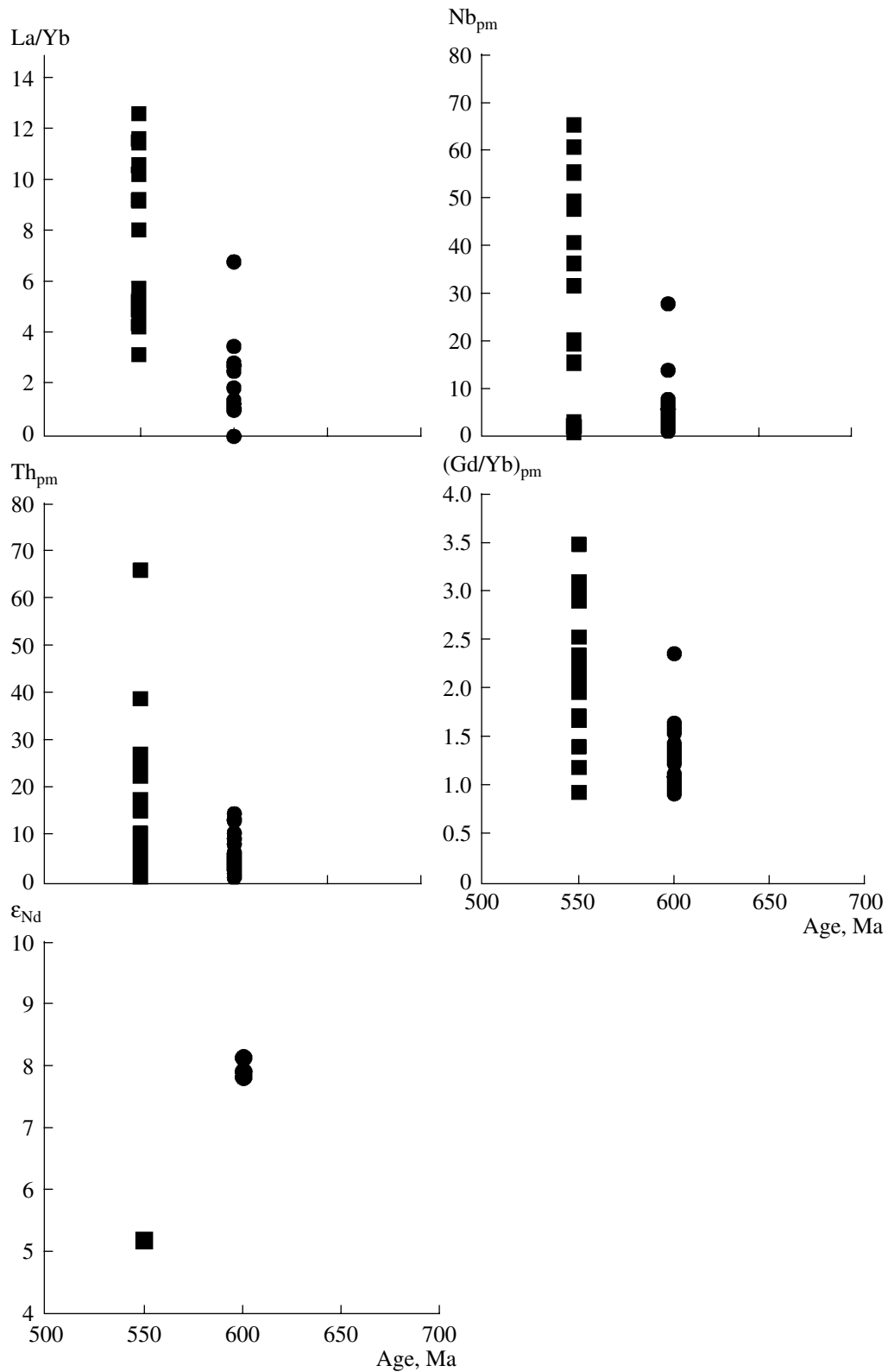


**Fig. 8.** Variations in  $La/Yb$ ,  $Nb$ ,  $Th$ ,  $(Gd/Yb)_{pm}$ , and  $\epsilon_{Nd}$  as functions of the age of intraplate tholeiites of the Paleo-Asian Ocean. Symbols are the same as in Fig. 3.

**Table 1.** Major- (wt %) and trace-element (ppm) compositions of basalts from the Kurai paleoseamount

Component	144	146	151	154	155	157	161	165	KR82	KR83	KR87	KR90	123	125	96-56-1	C-80A-04
SiO <sub>2</sub>	48.94	47.25	49.63	46.27	52.36	47.28	47.53	47.29	49.22	48.69	50.76	49.73	51.15	50.84	50.15	48.45
TiO <sub>2</sub>	1.77	1.84	1.09	2.36	1.84	1.53	1.78	1.65	2.05	2.42	2.07	1.68	1.32	1.66	1.51	1.86
Al <sub>2</sub> O <sub>3</sub>	13.49	13.67	15.80	12.90	14.17	15.72	16.15	14.60	14.24	14.39	16.36	13.84	13.47	14.83	14.57	12.21
Fe <sub>2</sub> O <sub>3</sub>	11.73	12.91	11.34	14.96	11.24	10.93	12.33	13.57	13.39	14.53	11.61	11.81	8.04	7.51	13.76	11.73
MnO	0.21	0.23	0.20	0.25	0.17	0.21	0.21	0.21	0.21	0.24	0.21	0.45	0.16	0.17	0.26	0.18
MgO	7.23	7.26	6.24	6.96	4.59	7.07	7.25	6.69	6.05	4.91	4.35	6.04	7.87	5.43	3.89	7.73
CaO	9.30	10.00	7.76	6.82	6.32	8.11	5.24	6.95	8.79	7.47	8.07	8.30	8.71	7.34	5.44	10.97
Na <sub>2</sub> O	3.86	3.32	3.28	5.18	4.76	3.85	4.44	4.28	3.92	3.88	5.00	5.27	3.04	4.58	5.76	2.09
K <sub>2</sub> O	0.35	0.29	0.37	0.49	0.70	0.74	0.44	0.44	0.21	1.45	0.45	0.12	1.34	0.71	0.71	0.30
P <sub>2</sub> O <sub>5</sub>	0.18	0.18	0.08	0.23	0.21	0.13	0.43	0.37	0.23	0.25	0.25	0.18	0.17	0.45	0.58	1.18
LOI	2.44	2.74	3.83	3.35	2.53	3.19	3.71	3.59					4.57	6.10	3.26	3.98
<b>Total</b>	99.5	99.7	99.6	99.8	98.9	98.7	99.5	99.6	98.3	98.2	99.1	97.4	99.8	99.6	99.9	100.7
<b>Mg#</b>	55.21	52.93	52.39	48.20	44.96	56.40	54.04	49.65	47.47	40.34	42.83	50.56	66.19	59.12	36.12	54.26
<b>La</b>	5.30	5.70	7.00	6.50	5.90	7.50	8.00	7.20	6.08	5.40	6.59	4.51	7.0	8.0	11	13
<b>Ce</b>	16.0	16.5	20.0	15.5	18.5	18.6	20.6	16.6	19.05	16.15	20.44	13.76	16.5	18	25	29
<b>Nd</b>	14.90	13.20	14.10	12.30	17.90	10.30	15.60	11.40	3.26	2.74	3.50	2.39	10.20	14	16	20
<b>Sm</b>	5.05	4.40	4.90	4.70	5.94	3.62	4.20	3.60	17.35	14.63	18.37	12.83	2.70	4.3	5.2	5.1
<b>Eu</b>	1.70	1.70	1.80	1.65	1.75	1.80	1.88	1.77	2.04	1.82	1.97	1.50	0.90	1.6	2.0	1.4
<b>Gd</b>	6.90								7.97	6.48	3.05	6.10				5.4
<b>Tb</b>	1.28	1.09	1.06	0.94	1.11	0.74	0.80	0.74	1.44	1.14	1.47	1.11	0.48	0.95	1.10	0.83
<b>Yb</b>	5.10	5.00	5.00	3.40	4.70	2.70	2.90	2.80	5.97	4.12	6.20	4.48	2.00	2.80	3.80	1.9
<b>Lu</b>	0.73	0.80	0.80	0.60	0.77	0.40	0.43	0.41	0.90	0.62	0.93	0.68	0.33	0.41	0.55	0.25

**Table 1.** (Contd.)

Component	144	146	151	154	155	157	161	165	KR82	KR83	KR87	KR90	123	125	96-56-1	C-80A-04
<b>Cr</b>		106	113	61	29.2	33.9	38.9	41.7					154	12.5		226
<b>Co</b>	55	53	48	52	38	38	39	40					42	30	48	62
<b>Ni</b>	51	41	38.9	21.7	22.9	7	22.2	14.3	39	14	23	42	96	7.4		105
<b>V</b>		326	362	417	337	307	469	349					89	135		
<b>Rb</b>	2.8	3.1	7.9	5.5	6.8	6.3	6.5	5.8	3.4	10.2	4.4	1.5	10.4	11.4	15.0	6.5
<b>Sr</b>	245.8	211	368	148	171	327	475	514	189	125	361	252	315.0	405.0	560	112
<b>Ba</b>	50	10	160	70	100	260	600	70	57	160	177	98	200	270	480	141
<b>Ta</b>	0.34	0.22	0.22	0.23	0.20	0.21	0.21	0.16	0.15	0.16	0.17	0.10	0.53	0.17	0.25	1.23
<b>Nb</b>	4.7	4.0	4.2	5.1	4.5	3.7	4.3	3.1	3.0	3.3	3.3	1.8	9.9	3.0	4.0	20.0
<b>Zr</b>	157	157	177	137	186	78	99	72	173	133	189	132	96	69	108	157
<b>Hf</b>	4	3.6	3.9	2.9	3.9	1.9	2.1	1.6	4.5	3.5	5	3.6	2	2.1	2	3.8
<b>Th</b>	0.31	0.25	0.3	0.35	0.25	0.45	0.5	0.4	0.3	0.3	0.5	0.7	0.55	0.5	0.9	1.11
<b>Y</b>	53	58	63	48.8	61	35.2	38.2	32.6	37	50	48	42	22.9	29.9	40	42.5
<b>U</b>	0.19	0.2	0.32	0.05	0.04	0.2	0.28	0.13					0.27	0.24		0.38
<b>Zr/Nb</b>	33	39	42	27	41	21	23	24	58	40	58	74	10	23	27	8
<b>(La/Sm)<sub>n</sub></b>	0.66	0.82	0.90	0.87	0.81	1.10	1.20	1.26	0.67	0.72	0.69	0.64	1.63	1.17	1.33	1.67
<b>(Gd/Yb)<sub>n</sub></b>	1.08	0.94*	0.96*	1.28*	1.02*	1.35*	1.30*	1.21*	1.03	1.20	1.03	1.06	1.17*	1.52*	1.31*	2.21
<b>(La/Yb)<sub>n</sub></b>	0.71	0.77	0.95	1.29	0.85	1.88	1.86	1.74	0.69	0.89	0.72	0.68	2.37	1.93	1.96	4.8
<b>(Nb/La)<sub>pm</sub></b>	0.85	0.68	0.58	0.75	0.74	0.47	0.52	0.41	0.47	0.59	0.47	0.38	1.36	0.37	0.35	1.48
<b>(Th/La)<sub>pm</sub></b>	0.47	0.35	0.35	0.44	0.34	0.48	0.51	0.45	0.40	0.45	0.61	1.25	0.64	0.51	0.66	0.69
<b>(Nb/Th)<sub>pm</sub></b>	1.81	1.93	1.68	1.72	2.16	0.97	1.03	0.91	1.19	1.31	0.77	0.30	2.14	0.72	0.53	2.15
<b>Al<sub>2</sub>O<sub>3</sub>/TiO<sub>2</sub></b>	7.6	7.4	14.6	5.5	7.7	10.3	9.1	8.9	6.9	5.9	7.9	8.2	10.2	9.0	9.6	6.6

\* The (Gd/Yb)<sub>n</sub> values were calculated using model Gd\* values.

**Table 2.** Major- (wt %) and trace-element (ppm) compositions of basalts from the Katun' paleoseamount

Component	238/1	238/2	239	241	92-C-1	E4068	E4086	E4096	E4112	E4124	E4127	E4131	E4132	E4133
SiO <sub>2</sub>	45.40	46.20	44.20	48.50	52.32	45.45	49.64	43.63	47.55	46.00	45.08	45.43	45.88	45.78
TiO <sub>2</sub>	2.42	2.06	2.42	1.94	2.26	2.91	2.20	2.60	2.11	2.26	2.93	2.56	2.70	2.82
Al <sub>2</sub> O <sub>3</sub>	14.20	13.90	13.00	15.00	12.44	16.81	15.95	15.34	12.95	15.08	14.71	14.34	14.51	15.81
Fe <sub>2</sub> O <sub>3</sub>	13.90	12.40	15.50	10.80	11.11	15.07	12.65	12.72	11.51	13.02	13.09	13.93	13.31	14.26
MnO					0.10	0.22	0.23	0.20	0.17	0.20	0.19	0.18	0.20	0.20
MgO	7.20	8.70	6.53	8.37	6.19	4.92	3.47	7.94	7.34	7.17	6.47	6.04	6.40	5.58
CaO	11.02	10.33	10.79	7.80	7.60	4.95	4.20	8.31	8.62	9.57	9.34	9.31	8.26	6.60
Na <sub>2</sub> O	1.67	2.37	1.99	3.16	5.04	4.01	4.67	2.70	2.90	2.47	3.04	3.41	3.73	3.51
K <sub>2</sub> O	0.37	0.36	0.39	0.65	0.68	1.05	3.61	1.03	2.11	1.35	0.41	0.76	1.09	1.99
P <sub>2</sub> O <sub>5</sub>	0.18	0.18	0.24	0.17	0.29	0.70	0.64	0.36	0.20	0.28	0.41	0.72	0.49	0.45
LOI	4.05	3.81	5.03	4.35	2.76	3.76	3.00	4.87	4.50	2.64	4.29	3.14	3.50	3.24
<b>Total</b>	100.4	100.3	100.1	100.7	100.8	99.9	100.3	99.7	100.0	100.0	100.0	99.8	100.1	100.2
<b>Mg#</b>	50.9	58.4	45.7	60.8	52.7	39.5	35.4	55.5	56.1	52.4	49.7	46.4	49.0	43.9
<b>La</b>	12.6	10.6	14.2	9.5	13.0	23.6	44.2	25.2	9.7	18.2	18.9	67.8	24.9	27.2
<b>Ce</b>	27.0	25.0	30.0	22.0	29.0	50.0	83.6	50.3	22.7	37.6	40.0	114.7	49.1	54.1
<b>Nd</b>	17.0	18.0	20.0	14.5	20.0	29.4	43.4	27.7	15.0	21.6	23.6	52.8	26.7	29.8
<b>Sm</b>	5.3	5.4	6.0	4.3	5.4	7.9	10.6	7.1	4.4	5.7	6.4	11.7	6.8	7.6
<b>Eu</b>	1.7	1.6	1.9	1.5	1.4	2.8	2.8	2.2	1.5	1.6	2.2	3.2	2.3	2.3
<b>Gd</b>	5.8	6.1	6.4	4.6	5.7	6.8	9.9	6.2	5.9	4.0	7.4	8.5	8.3	6.9
<b>Tb</b>	0.9	0.9	1.1	0.8	0.8	1.1	1.6	1.0	0.9	0.7	1.1	1.3	1.2	1.1
<b>Yb</b>	2.4	2.4	2.7	2.2	2.1	2.2	3.8	2.2	1.7	2.0	2.1	2.3	2.0	2.7
<b>Lu</b>	0.3	0.3	0.4	0.3	0.3	0.3	0.5	0.3	0.2	0.3	0.3	0.3	0.3	0.4

**Table 2.** (Contd.)

Component	238/1	238/2	239	241	92-C-1	E4068	E4086	E4096	E4112	E4124	E4127	E4131	E4132	E4133
<b>Cr</b>	310	380	635	260		55	12	130	280	91	146	2	147	39
<b>Co</b>	54	51	48	45	63	44	24	63	38	52	44	51	41	45
<b>Ni</b>	43.8	43.1	42.0	40.1	184.0	21.6	15.5	40.1	30.0	40.9	37.2	34.9	31.6	31.3
<b>V</b>	317	269	263	238	120	493	501	254	213	616	380	314	520	4133
<b>Rb</b>	5	4	6	7	7	15	46	14	28	23	2	6	8	22
<b>Sr</b>	317	269	263	238	110.0	493	501	254	213	616	380	314	520	830
<b>Ba</b>	60	60	105	100	144	870	930	390	400	650	370		540	670
<b>Ta</b>	1.0	0.6	0.9	0.7	1	1.6	3.9	1.9	0.8	1.5	1.4	2.0	1.8	2.1
<b>Nb</b>	13.9	10.9	14.5	11.2	20	34.1	131.6	39.6	22.6	35.2	29.1	43.3	39.5	46.7
<b>Zr</b>	121	113	134	109	154	217	420	147	130	208	133	135	191	255
<b>Hf</b>	3.6	3.3	3.9	2.9	3.8	4.5	6.7	4.0	2.9	3.5	3.8	4.4	4.5	5.3
<b>Th</b>	0.9	0.5	0.8	0.6	1	1.5	3.3	2.1	0.6	1.4	1.3	5.6	1.9	2.3
<b>Y</b>	23	22	26	22	29	32	55	21	21	28	20	20	27	29
<b>U</b>					0.4	1.1	1.3	1.0	0.4	0.4	0.5	1.3	0.6	0.8
<b>Zr/Nb</b>	9	10	9	10	8	6	3	4	6	6	5	3	5	5
<b>(La/Sm)<sub>n</sub></b>	1.53	1.27	1.53	1.44	1	1.88	2.62	2.23	1.39	2.01	1.87	3.65	2.30	2.25
<b>(Gd/Yb)<sub>n</sub></b>	1.99	2.12	1.95	1.71	2.2	2.48	2.11	2.29	2.85	1.65	2.93	3.03	3.41	2.10
<b>(La/Yb)<sub>n</sub></b>	3.75	3.19	3.76	3.07	3.37	7.18	7.86	7.78	3.90	6.27	6.23	20.18	8.54	6.91
<b>(Nb/La)<sub>pm</sub></b>	1.06	0.99	0.98	1.14	1.5	1.39	2.87	1.51	2.24	1.86	1.48	0.62	1.53	1.65
<b>(Th/La)<sub>pm</sub></b>	0.51	0.46	0.51	0.43	0.65	0.51	0.60	0.67	0.50	0.62	0.56	0.67	0.62	0.68
<b>(Nb/Th)<sub>pm</sub></b>	2.07	2.17	1.92	2.67	2.27	2.71	4.75	2.25	4.49	3.00	2.67	0.92	2.48	2.42
<b>Al<sub>2</sub>O<sub>3</sub>/TiO<sub>2</sub></b>	5.9	6.7	5.4	7.7	3.4	5.8	7.3	5.9	6.1	6.7	5.0	5.6	5.4	5.6

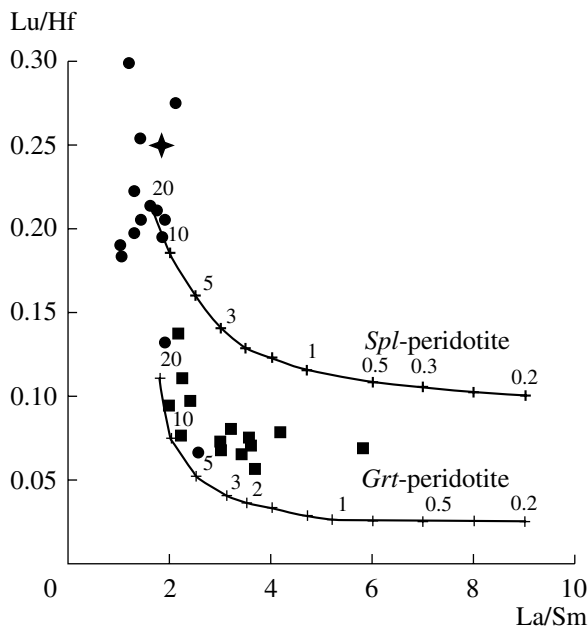


**Fig. 9.** Curves of partial melting (from 0.01 to 20 %) of spinel and garnet peridotites (Regelous et al., 2003). Since the Kurai basalts are probably derived from mixed garnet and spinel peridotite sources, their low La/Sm and high Lu/Hf values indicate relatively high degrees of melting within the spinel stability field and a source with a La/Sm ratio approaching that of the primitive mantle (Sun and McDonough, 1989). The asterisk corresponds to the primitive mantle composition. Other symbols are the same as in Fig. 3.

Thus, the temporal variations in the composition of lavas from the Kurai and Katun' paleoseamounts could result from varying degrees of nonequilibrium melting in the compositionally and structurally heterogeneous column of the mantle plume. It is supposed that the column is composed of a more refractory matrix consisting of the depleted upper mantle material and less refractory heterogeneities (Phipps Morgan and Morgan, 1999; Hoernle et al., 2000; etc.). The nature of these heterogeneities in the mantle column is still unclear, but it is supposed that they are domains affected by a thermochemical mantle plume and enriched with low-melting components from the lower mantle (LREE and LILE) and Nb (Dobretsov et al., 2006; Allègre and Turcotte, 1986).

The varying degrees of melting in a heterogeneous mantle column could result from the different thickness of the overlying lithosphere (Fig. 10). During progressive melting of such a heterogeneous mantle, the melts formed beneath the growing, but still thin lithosphere will have lower concentrations and ratios of incompatible elements (e.g., La, Nb, and Th) (Phipps Morgan, 1999). Therefore, we suppose that the more depleted composition of the Kurai lavas resulted from the melting of the relatively refractory depleted component of the upper mantle in the ascending plume column (Fig. 10a). The younger Katun' lavas were formed from

a melt produced by lower degree melting in a shorter mantle column beneath a thicker oceanic lithosphere. As a result, this melt contained less material from the refractory matrix (Fig. 10b) but more material from the enriched mantle heterogeneities.

A similar tendency providing evidence for a change in the geochemistry of plume magmatism was reported for other seamount chains: (1) the Ninetyeast Ridge (from ~90 to 38 Ma) and the Kerguelen Archipelago/Plateau (from ~45 Ma to Recent) in the Indian Ocean above the Kerguelen plume (Gautier et al., 1990; Frey and Weis, 1995; etc.); (2) the Easter volcanic chain in the eastern Pacific (from the Recent volcanoes of Easter Island to seamounts with an age of 30 Ma in its eastern part; Cheng et al., 1999 and others); (3) the Emperor–Hawaii Seamount Chain with lavas varying in age from 85 Ma in its northwestern end to 42 Ma in the east (Regelous and Hofmann, 1999; Keller et al., 2000; Regelous et al., 2003).

Finally, it should be emphasized that variations in the geochemical composition of seamount lavas are related to the thickening of the oceanic lithosphere, which is an important factor controlling the degree of mantle melting above a plume and, consequently, melt composition. The results reported by Ellam (1992), Regelous et al. (2003), and Ito and Mahoney (2005) suggest the dependence of intraplate basalt composition on lithosphere thickness, and this effect can be observed only in island chains with an age range of no more than 80 Myr. The relationships revealed by these authors were used in this paper to elucidate the reason for the compositional differences between the intraplate volcanics of the Kurai (600 Ma) and Katun' (550–530 Ma) paleoseamounts in the southwestern Paleo-Asian Ocean, whose basalt–sedimentary sequences are accessible now for investigation in the Kurai and Katun' accretionary zones of Gorny Altai, southwestern Siberia.

## CONCLUSIONS

(1) The obtained petrochemical and isotopic data for volcanic rocks from the fragments of two paleoseamounts of the Paleo-Asian Ocean shed light on the evolution of intraplate oceanic magmatism over 50 Myr (from 600 to 550 Ma) and showed that the geochemical and isotopic characteristics of lavas changed significantly during that period.

(2) The lavas of the older Kurai Paleoseamount (~600 Ma) have more depleted trace-element and isotopic characteristics compared with the younger lavas of the Katun' Paleoseamount (~550 Ma) and higher initial  $\epsilon_{Sr}$  values compared with the oceanic tholeiites of the Emperor–Hawaii Seamount Chain and Hawaiian Islands, which is related to the postmagmatic alteration of the Kurai lavas. The Kurai lavas correspond to the Hawaiian rocks with respect to  $\epsilon_{Nd}$  values. The initial  $\epsilon_{Sr}$  values of the tholeiites of the Katun' Paleoseamount

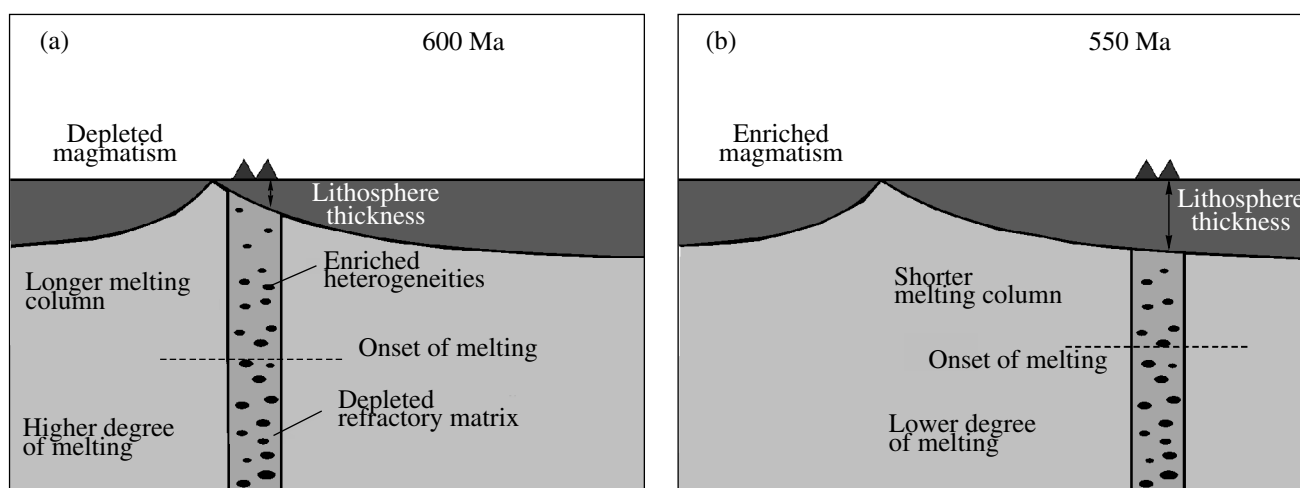


**Fig. 10.** Cartoon illustrating the influence of lithosphere thickness on the incompatible element composition of Late Proterozoic–Early Cambrian basalts of the Paleo-Asian Ocean, modified after Regelous et al. (2003). (a) The depleted lavas of the Kurai paleoseamount are derived by relatively high degrees of melting of a heterogeneous mantle; the major portion of refractory material depleted in incompatible elements was involved in the melting of an ascending mantle plume beneath a younger and thinner lithosphere (600 Ma). (b) In contrast, the basalts of the Katun' Paleoseamount were derived beneath a more mature and thicker oceanic lithosphere (550–530 Ma); the average degree of melting was lower, and the contents of incompatible elements appeared to be higher owing to the less refractory material of mantle heterogeneities.

are on average higher, whereas the  $\epsilon_{\text{Nd}}$  values are on average lower than those of the EHC lavas; however, the composition of the Katun' tholeiite plots within the field of the Hawaiian tholeiites in the  $\epsilon_{\text{Sr}}-\epsilon_{\text{Nd}}$  diagram.

(3) The trace-element and isotopic characteristics of the lavas vary depending on the age of the underlying lithosphere of the Paleo-Asian Ocean during basalt eruption. The older Kurai lavas probably erupted onto the relatively young and thin lithosphere of the Paleo-Asian Ocean closer to the spreading axis and have more depleted incompatible element and isotope compositions. In contrast, the younger Katun' lavas erupted onto a thicker lithosphere and have more enriched compositions.

(4) The major- and trace-element characteristics of the lavas of the Kurai Paleoseamount suggest that they were formed at higher degrees of mantle melting and lower pressures compared with the younger lavas of the Katun' Paleoseamount.

(5) By analogy with the Emperor–Hawaii Seamount Chain, it can be supposed that the temporal variations in the geochemical characteristics of the intraplate magmatism of the Paleo-Asian Ocean could be controlled by the variable degree of melting of a compositionally heterogeneous mantle and different thickness of the oceanic lithosphere at the moment of melt generation. During the Ediacaran, the mantle plume was located beneath a thinner lithosphere, probably closer to the spreading axis, and the relatively high degrees of melting produced the Kurai melts with more depleted trace-element signatures owing to the higher contribution to the melt from the refractory depleted material of the upper mantle. The Katun' melts were derived in the

Early Cambrian beneath a thicker lithosphere and at lower degrees of melting, which resulted in their enrichment in the components of less refractory lower mantle heterogeneities.

#### ACKNOWLEDGMENTS

The material for this paper was collected during fieldwork in Gorny Altai in 1995–2004. The author thanks her colleagues from the laboratory of geodynamics and magmatism of the Institute of Geology and Mineralogy, Siberian Branch, Russian Academy of Sciences, primarily, the head of the laboratory Dr. M.M. Buslov for cooperation in the field and discussion of the manuscript; the chiefs of analytical groups of the Institute of Geology and Mineralogy, Siberian Branch, Russian Academy of Sciences V.A. Bobrov, A.D. Kireev, and S.V. Palesskii for the analysis of major and trace elements by the INAA, XRF, and ICP MS techniques; Dr. Yu.A. Kostitsyn (Vernadsky Institute of Geochemistry and Analytical Chemistry, Russian Academy of Sciences) for isotope analyses; and Dr. S.A. Silantyev (Vernadsky Institute of Geochemistry and Analytical Chemistry, Russian Academy of Sciences) for helpful comments, which greatly improved the manuscript.

This study was financially supported by international grant no. 07-05-91211 of the Russian Foundation for Basic Research and the Japan Society for the Promotion of Science.

## REFERENCES

1. C. J. Allegre and D. L. Turcotte, "Implications of a Two-Component Marble-Cake Mantle," *Nature* **323**, 123–127 (1986).
2. A. R. Basu and B. E. Faggart, "Temporal Isotopic Variation in the Hawaiian Mantle Plume: the Lanai Anomaly, the Molokai Fracture Zone, and a Seawater-Altered Lithospheric Component in Hawaiian Volcanism," in *Earth Processes: Reading the Isotopic Code*, Ed. by A. Basu and S. R. Hart, Geophys. Monogr., Am. Geophys. Union **95**, 149–159 (1996).
3. W. H. Berger and E. L. Winterer, "Plate Stratigraphy and the Fluctuating Carbonate Line in Pelagic Sediments," in *On Land and under the Sea*, Ed. by K. J. Hsu and H. C. Jenkyns, Int. Ass. Sedimentologists, No. 1, 11–98 (1974).
4. N. A. Berzin, R. G. Coleman, N. L. Dobretsov, et al., "Geodynamic Map of the Western Part of the Paleasian Ocean," *Geol. Geofiz.* **35** (7–8), 8–28 (1994).
5. M. M. Buslov, I. Yu. Saphonova, T. Watanabe, et al., "Evolution of the Paleo-Asian Ocean (Altai-Sayan Region, Central Asia) and Collision of Possible Gondwana-Derived Terranes with the Southern Marginal Part of the Siberian Continent," *Geosci. J.* **5**, 203–224 (2001).
6. M. M. Buslov, T. Watanabe, I. Yu. Saphonova, et al., "Vendian–Cambrian Island Arc System of the Siberian Continent in Gorny Altai (Russia, Central Asia)," *Gondwana Res.* **5**, 781–800 (2002).
7. Q. C. Cheng, K.-H. Park, J. D. Macdougall, et al., "Isotopic Evidence for a Hot Spot Origin of the Louisville Seamount Chain," in *Seamounts, Islands and Atolls*, Ed. by B. H. Keating, P. Fryer, R. Batiza, and G. W. Boehlert, Geophys. Monogr. Am. Geophys. Union **43**, 283–296 (1987).
8. Q. C. Cheng, J. D. Macdougall, and P. Zhu, "Isotopic Constraints on the Easter Seamount Chain Source," *Contrib. Mineral. Petrol.* **135**, 225–233 (1999).
9. A. P. Dickin, *Radiogenic Isotope Geology* (University Press, Cambridge, 1995).
10. N. L. Dobretsov, N. A. Berzin, and M. M. Buslov, "Opening and Tectonic Evolution of the Paleo-Asian Ocean," *Int. Geol. Rev.* **35**, 335–360 (1995).
11. N. L. Dobretsov, M. M. Buslov, I. Yu. Safonova, and D. A. Kokh, "Fragments of Oceanic Islands in the Structure of the Kurai and Katun' Accretionary Wedges of Gorny Altai," *Geol. Geofiz.* **45**, 1381–1403 (2004).
12. N. L. Dobretsov, V. A. Simonov, M. M. Buslov, and A. V. Kotlyarov, "Magmatism and Geodynamics of the Paleasian Ocean during the Vendian–Cambrian Stage of Its Evolution," *Geol. Geofiz.* **46**, 952–967 (2005).
13. N. L. Dobretsov, A. A. Kirdyashkin, A. G. Kirdyashkin, et al., "Parameters of Hotspots and Thermochemical Plumes during Their Ascent and Eruption," *Petrologiya* **14**, 508–523 (2006) [*Petrology* **14**, 477–491 (2006)].
14. C. Dupuy, P. Vidal, R. C. Maury, et al., "Basalts from Mururoa, Fangataufa and Gambier Islands (French Polynesia): Geochemical Dependence on the Age of the Lithosphere," *Earth Planet. Sci. Lett.* **117**, 89–100 (1993).
15. R. M. Ellam, "Lithospheric Thickness as a Control on Basalt Geochemistry," *Geology* **20**, 153–156 (1992).
16. F. A. Frey and D. Weis, "Temporal Evolution of the Kerguelen Plume: Geochemical Evidence from 38 to 82 Ma Lavas Forming the Ninetyeast Ridge," *Contrib. Mineral. Petrol.* **121**, 12–28 (1995).
17. T. I. Frolova and I. A. Burikova, *Magmatic Associations of Present-Day Tectonic Settings* (Mosk. Gos. Univ., Moscow, 1997) [in Russian].
18. I. Gautier, D. Weis, J.-P. Mennessier, et al., "Petrology and Geochemistry of the Kerguelen Archipelago Basalts (South Indian Ocean): Evolution of the Mantle Sources from Ridge to Intraplate Position," *Earth Planet. Sci. Lett.* **100**, 59–76 (1990).
19. A. S. Gibsher, S. V. Esin, A. E. Izokh, et al., "Cambrian Diopside-Bearing Basalts of the Cheposhskaya Zone, Gorny Altai: Model of Hybrid Magma Fractionation in Intermediate Chambers," *Geol. Geofiz.* **38**, 1760–1772 (1997).
20. I. V. Gordienko, A. V. Filimonov, O. R. Minina, et al., "Dzhida Island Arc System of the Paleasian Ocean: Structure and Main Stages of the Geodynamic Evolution in the Vendian–Paleozoic," *Geol. Geofiz.* **48**, 120–141 (2007).
21. K. M. Haase, "The Relationship between the Age of the Lithosphere and the Composition of Oceanic Magmas: Constrains on Partial Melting, Mantle Sources and the Thermal Structure of the Plates," *Earth Planet. Sci. Lett.* **144**, 75–92 (1996).
22. K. Hoernle, R. Werner, J. Phipps Morgan, et al., "Existence of Complex Spatial Zonation in the Galapagos Plume for at Least 14 M.Y.," *Geology* **28**, 435–438 (2000).
23. A. W. Hofmann, "Mantle Geochemistry: the Message from Oceanic Volcanism," *Nature* **385**, 219–229 (1997).
24. A. W. Hofmann and K. P. Jochum, "Source Characteristics Derived from Very Incompatible Trace Elements in Mauna Loa and Mauna Kea Basalts, Hawaii Scientific Drilling Project," *J. Geophys. Res.* **101**, 11831–11839 (1996).
25. A. W. Hofmann and W. M. White, "Mantle Plumes from Ancient Oceanic Crust," *Earth Planet. Sci. Lett.* **57**, 421–436 (1982).
26. Y. Isozaki, Sh. Maruyama, and F. Fukuoka, "Accreted Oceanic Materials in Japan," *Tectonophysics* **181**, 179–205 (1990).
27. G. Ito and J. J. Mahoney, "Flow and Melting of a Heterogeneous Mantle. 2. Implications for a Chemically Non-Layered Mantle," *Earth Planet. Sci. Lett.* **230**, 47–63 (2005).
28. R. A. Keller, M. R. Fisk, and W. M. White, "Isotopic Evidence for Late Cretaceous Plume–Ridge Interaction at the Hawaiian Hotspot," *Nature* **405**, 673–676 (2000).
29. A. I. Khanchuk, A. P. Nikitina, I. V. Panchenko, et al., "Paleozoic and Mesozoic Guyots of the Sikhote-Alin and Sakhalin," *Dokl. Akad. Nauk SSSR* **307**, 186–190 (1989).
30. T. Komiya, Sh. Maruyama, T. Hirata, and S. Nohda, "Petrology and Geochemistry of MORB and OIB in the Mid-Archean North Pole Region, Pilbara Craton, Western Australia: Implications for the Composition and Temperature of the Upper Mantle at 3.5 Ga," *Int. Geol. Rev.* **44**, 988–1016 (2002).

31. J. J. Mahoney, R. Frei, M. L. Tejada, et al., "Tracing the Indian Ocean Mantle Domain through Time: Isotopic Results from Old West Indian, East Tethyan, and South Pacific Seafloor," *J. Petrol.* **39**, 1285–1306 (1998).
32. Sh. Maruyama, "Plume Tectonics," *J. Geol. Soc. Japan* **100** (1), 24–49 (1994).
33. W. S. McKerrow, C. R. Scotese, and M. D. Brosier, "Early Cambrian Reconstruction," *J. Geol. Soc. London* **149**, Part 4, 589–606 (1992).
34. W. J. Morgan, "Convection Plumes in the Lower Mantle," *Nature* **230**, 42–43 (1971).
35. T. Ota, A. Utsunomiya, Yu. Uchio, et al., "Geology of the Gorny Altai Subduction–Accretion Complex, Southern Siberia: Tectonic Evolution of an Ediacaran–Cambrian Intra-Oceanic Arc–Trench System," *J. Asian Earth Sci.* **30**, 666–695 (2007).
36. I. A. Phedorin, V. A. Bobrov, E. P. Chebykin, et al., "Comparison of Synchrotron Radiation X-Ray Fluorescence with Conventional Techniques for the Analysis of Sedimentary Samples," *Geostand. Newslett.* **24**, 205–216 (2000).
37. J. Phipps Morgan, "Isotope Topology of Individual Hotspot Basalt Arrays: Mixing Curves or Melt Extraction Trajectories?," *Geochem. Geophys. Geosys.* **1**, GC000004 (1999).
38. J. Phipps Morgan and W. J. Morgan, "Two-Stage Melting and the Geochemical Evolution of the Mantle: A Recipe for Mantle Plum-Pudding," *Earth Planet. Sci. Lett.* **170**, 215–239 (1999).
39. W. C. Pitman and M. Talwani, "Sea-Floor Spreading in the North Atlantic," *Geo-Mar. Lett.* **83**, 619–646 (1972).
40. A. Polat, R. Kerrich, and D. Wyman, "Geochemical Diversity in Oceanic Komatiites and Basalts from the Late Archean Wawa Greenstone Belts, Superior Province, Canada: Trace Element and Nd Isotope Evidence for a Heterogeneous Mantle," *Precambrian Res.* **94**, 139–173 (1999).
41. A. A. Postnikov and A. A. Terleev, "Stratigraphy of the Neoproterozoic of the Altai–Sayan Fold Area," *Geol. Geofiz.* **45**, 295–309 (2004).
42. M. Regelous and A. W. Hofmann, "Geochemistry of Lavas from the Emperor Seamounts, and the Geochemical Evolution of Hawaiian Magmatism Since 85 Ma," *EOS Transactions, Am. Geophys. Union* **80**, F1102 (1999).
43. M. Regelous, A. W. Hofmann, W. Abouchami, et al., "Geochemistry of Lavas from the Emperor Seamounts, and the Geochemical Evolution of Hawaiian Magmatism from 85 to 42 Ma," *J. Petrol.* **44**, 113–140 (2003).
44. P. W. Reiners, "Reactive Melt Transport in the Mantle and Geochemical Signatures of Mantle-Derived Magmas," *J. Petrol.* **39**, 1039–1061 (1998).
45. L. N. Repina and E. V. Romanenko, *Trilobites and the Lower Cambrian Stratigraphy of the Altai* (Nauka, Moscow, 1978) [in Russian].
46. I. Yu. Safonova, *Extended Abstracts of Candidate's Dissertation in Geology and Mineralogy* (NP AI "Geo", Novosibirsk, 2005) [in Russian].
47. I. Yu. Safonova, M. M. Buslov, K. Iwata, et al., "Fragments of Vendian–Early Carboniferous Oceanic Crust of the Paleo-Asian Ocean in Foldbelts of the Altai-Sayan Region of Central Asia: Geochemistry, Biostratigraphy and Structural Setting," *Gondwana Res.* **7**, 771–790 (2004).
48. V. A. Simonov, N. L. Dobretsov, and M. M. Buslov, "Boninite Series in the Structures of the Paleoasian Ocean," *Geol. Geofiz.* **35** (7-8), 182–199 (1994).
49. R. A. Stern, E. C. Syme, and S. B. Lucas, "Geochemistry of 1.9 Ga MORB- and OIB-Like Basalts from the Amisk Collage, Fin Flon Belt, Canada: Evidence for an Intra-oceanic Origin," *Geochim. Cosmochim. Acta* **59**, 3131–3154 (1995).
50. S. Sun and W. F. McDonough, "Chemical and Isotopic Systematics of Oceanic Basalts: Implications for Mantle Composition and Processes," in *Magmatism in the Ocean Basins*, Ed. by A. D. Saunders and M. J. Norry, *Geol. Soc. London Spec. Publ.* **42**, 313–345 (1989).
51. A. A. Terleev, "Stratigraphy of the Vendian–Cambrian Deposits of the Katun' Anticline (Gorny Altai)," in *Late Precambrian and Early Paleozoic of Siberia*, Ed. by V. V. Khomentovskii (OIGGiM, Novosibirsk, 1991), pp. 82–106 [in Russian].
52. Yu. Uchio, Yu. Isozaki, T. Ota, et al., "The Oldest Mid-Oceanic Carbonate Buildup Complex: Setting and Lithofacies of the Vendian (Late Neoproterozoic) Baratal Limestone in the Gorny Altai Mountains, Siberia," *Proc. Japan Acad.* **80** (9), 422–428 (2004).
53. I. P. Voinova, S. V. Zybrev, and V. S. Prikhod'ko, "Petrochemical Features of the Early Cretaceous Within-Plate Oceanic Volcanic Rocks of the Kiselev–Manoiminskii Terrane, Northern Sikhote Alin," *Tikhookean. Geol.*, No. 6, 83–96 (1994).
54. R. V. White, J. Tarney, A. C. Kerr, et al., "Modification of an Oceanic Plateau, Aruba, Dutch Caribbean: Implications for the Generation of Continental Crust," *Lithos* **46**, 43–68 (1999).
55. V. V. Yarmolyuk and V. I. Kovalenko, "Deep Geodynamics and Mantle Plumes: Their Role in the Formation of the Central Asian Fold Belt," *Petrologiya* **11**, 556–586 (2003) [*Petrology* **11**, 504–531 (2003)].
56. V. V. Yarmolyuk, V. I. Kovalenko, and M. I. Kuz'min, "North Asian Superplume Activity in the Phanerozoic: Magmatism and Geodynamics," *Geotektonika*, No. 5, 3–29 (2000) [*Geotectonics* **34**, 343–366 (2000)].
57. L. P. Zonenshain, M. I. Kuz'min, and L. M. Natapov, *Tectonics of the Lithospheric Plates of the USSR Territory* (Nedra, Moscow, 1990) [in Russian].